A methodology for automated quantitative microstructural analysis of transmission electron micrographs

D. T. Carpenter,[a] J. M. Rickman, and K. Barmak
Department of Materials Science and Engineering, Lehigh University, 5 East Packer Avenue, Bethlehem, Pennsylvania 18015

(Received 28 May 1998; accepted for publication 13 August 1998)

It is generally recognized that proper quantification of microstructural behavior is necessary for the optimization of materials properties. In the specific case of polycrystalline thin films, transmission electron microscopy (TEM) is required for microstructural interrogation due to the small (nm–μm) inherent length scales in these systems. While a meaningful study requires large grain populations, typical data sets are relatively small due to the need for human interpretation of the contrast in TEM micrographs. To overcome this limitation, a general methodology has been developed to fully automate the grain boundary identification procedure by using a combination of both conventional and newly developed image processing algorithms to extract and combine information from multiple, optimized TEM micrographs. This technique has been validated by systematically analyzing microstructures of thin Al films, as obtained from TEM micrographs, and comparing these results with those obtained by a conventional, manual approach. Indeed, a statistical analysis shows that the agreement between these two methods is quite good. We further show that based upon a large population (8185 grains) one can estimate the number of grains required to draw meaningful conclusions about this microstructure. While the emphasis of this work is on TEM image processing, the techniques developed here are expected to be sufficiently general and flexible so as to be applicable to other (e.g., focused-ion beam) microscopies. © *1998 American Institute of Physics.* [S0021-8979(98)02023-4]

I. INTRODUCTION

The microstructure of polycrystalline systems is known to have a profound effect on their mechanical, electronic, and magnetic properties, and therefore quantitative stereological analysis of microstructures is becoming increasingly important.[1] Proper characterization includes information not only about the size and shape of constituent grains, but also the geometry of the associated grain boundaries.[2–4] Depending on the length scale of the system under consideration, various experimental techniques, including both light (μm to mm) and electron (nm to μm) microscopy have been employed in microstructural interrogation. In systems of limited spatial dimensionality on the order of 1 nm to 1 μm (e.g., thin metallic films), the inherent length scales typically necessitate the use of transmission electron microscopy (TEM) in order to resolve the details of the grain structure.[5] When one considers that the functionalities of microelectronic devices, information storage media, read/write heads, sensors, and displays all depend critically on the microstructure of thin metallic films, it is clear that proper characterization is of paramount importance in these systems.

Unfortunately, the contrast characteristic of TEM images is often so complex that the identification of boundaries between grains is problematic, even for an experienced eye. This is illustrated in Fig. 1, showing a TEM micrograph of an as-deposited 100 nm Al thin film, with a particularly simple microstructure in which columnar grains span the thickness of the film. The main difficulty is that there are multiple sources of contrast which may be active, and not easily deconvoluted, resulting in image contrasts which often defy simple interpretation. This being the case, conventional image processing algorithms are of very limited utility since they are designed primarily to deal with simpler images. Consequently, the state-of-the-art in microstructural analysis from TEM images involves human intervention either to trace the grain boundaries or to identify grain diameters in a micrograph. The tedium associated with such an effort has meant that, in practice, very few workers have sought to collect the volume of experimental data necessary to properly quantify microstructural characteristics of interest. Thus, it is fair to say that most microstructural studies to date have been necessarily semiquantitative in nature owing to a small population of analyzed grains, typically on the order of 100 grains and in rare cases as many as 2000 grains.[6–9]

With these limitations in mind, the objective of this article is to present a practical scheme for the acquisition of microstructural information from a statistically significant population of grains, as extracted from TEM images. It is important to note here that we have incorporated many tried and tested techniques from the substantial existing literature in the field of image analysis.[10–14] However, as we will discuss below, the problems peculiar to TEM micrographs necessitate the creation of new, complementary algorithms. Thus, the work presented here focuses on the implementation of a suite of techniques, both old and new, in optimal combination to achieve the goal of systematically analyzing large quantities of microstructural data, especially (though not exclusively) in thin metal film systems. While the emphasis here is on analysis of TEM images, the methods employed

[a]Original micrographs are available from the authors upon request.

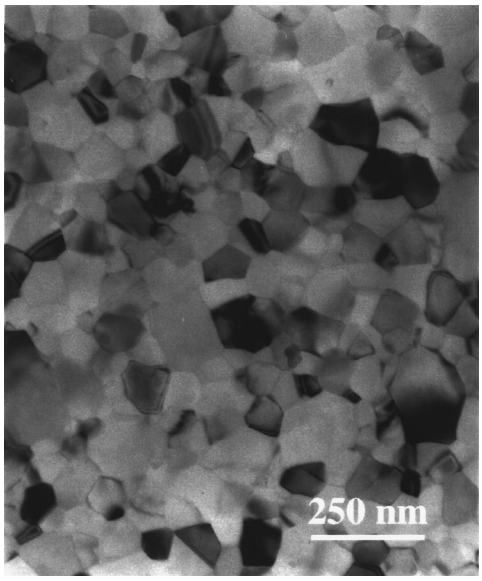

FIG. 1. Bright-field TEM micrograph showing the typical microstructure of a 100 nm as-deposited Al film (*courtesy G. A. Lucadamo*).

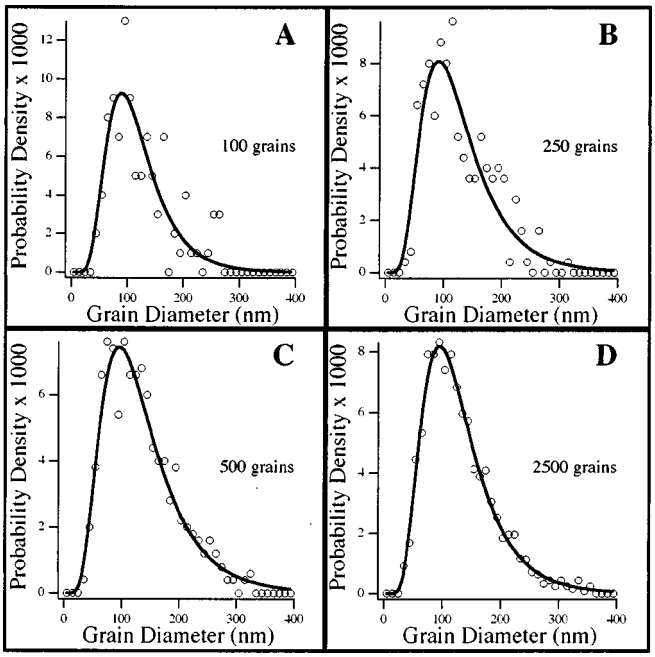

FIG. 2. Grain size histograms extracted from hand-traced micrographs with populations of (A) 100 grains, (B) 250 grains, (C) 500 grains, and (D) 2500 grains, fitted to lognormal distributions shown as smooth curves. Larger grain populations exhibit reduced noise and improved goodness of fit.

are sufficiently general so as to be applicable to a wide variety of images obtained by various techniques, e.g., focused ion beam (FIB) microscopy.

The organization of this article is as follows. In Sec. II we discuss the requirements for obtaining meaningful microstructural information and the difficulties of obtaining this information from TEM images. Section III describes the experimental procedures for the acquisition and analysis of TEM micrographs from a thin Al film. Section IV comprises a general overview of the image processing methodology followed by a description of newly developed algorithms. Section V contains results and discussion, and Sec. VI concludes the article.

II. BACKGROUND

As noted previously, the acquisition of rather limited grain populations has hampered quantitative microstructural analyses. Before discussing the application of image processing techniques to the examination of TEM images, it is first helpful to obtain a rough estimate of the number of grains that must be analyzed in order to obtain meaningful microstructural information. As a specific illustration, consider the grain size histograms from various grain populations, measured by hand from TEM micrographs of an annealed Al thin film, as shown in Fig. 2. For the purpose of comparison, each histogram has been fitted to the typically assumed lognormal distribution. While it is sometimes difficult to assess whether the histogram is a satisfactory representation of the underlying grain size distribution, it should be pointed out here that typical experimental analyses are based on several hundred grains, and the fits in Fig. 2 suggest that such a small sampling is insufficient for microstructural quantification. Although the lognormal fits result in similar values for the mean and standard deviation regardless of sample size, the scatter in the data is much more pronounced for the smaller samples, which can be very significant when the higher moments of the distribution are of interest. While the acquisition of additional grain statistics may seem like a relatively small effort, it must be remembered that such an increase will require more micrographs, and more importantly, concomitant increases in the human effort required for conventional manual analysis. The requirement of human intervention to identify microstructural features is clearly the rate-limiting step in this process, suggesting that further progress requires some type of automation.

The difficulties encountered in attempting to apply conventional image processing techniques to typical TEM micrographs can perhaps best be illustrated by examining Fig. 3. The grain structure of an as-deposited 100 nm Al thin film is shown in Fig. 3(A), and the result of typical image processing is shown in Fig. 3(B). The particular processing steps applied consisted of median filtering, Sobel edge detection, manual thresholding, skeletonization, dilation, erosion, and closing (these operations are described in Appendix B). It is

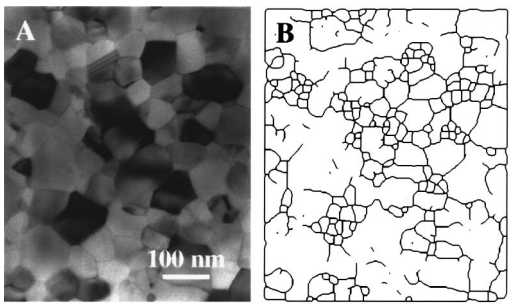

FIG. 3. (A) Typical bright-field TEM micrograph of a 100 nm Al film showing contrast ambiguities. (B) Edges located in the same image using a typical sequence of conventional image processing routines, showing a large number of unreliable features.

clear that the resulting analyzed microstructure in Fig. 3(B) is a poor representation of the grain boundaries in Fig. 3(A). A closer examination of the original micrograph reveals that feature identification is limited by problems associated with contrast. Specifically, many real boundaries show only very faint contrast and are therefore not detected, while a large number of spurious features show strong contrast and result in the appearance of many small, erroneous grains in the processed image. While a human observer is often more successful at locating grain boundaries given his/her ability to integrate spatially nonlocal, topological information, he/she is still limited by these inherent contrast ambiguities.

Clearly, before a fully automated approach can be developed this spurious information must be eliminated, or at least minimized. Most efforts concentrate primarily on the improvement of image processing algorithms to do this, with some success. However, when it is difficult for a person to differentiate between real features and spurious ones (as is often the case with TEM images), it becomes exceedingly difficult to define the rules which would allow a computer to do so. Therefore, it is perhaps a more reasonable goal to improve the quality of the starting images and minimize such spurious features before processing is even attempted. This should substantially reduce the complexity of subsequent image processing operations without loss of information. Our strategy for improving image quality prior to processing will be discussed in detail in Sec. III.

III. EXPERIMENTAL PROCEDURES

Plan view TEM and scanning transmission electron microscopy (STEM) images of the microstructure of as-deposited Al thin films were used in the testing and development of the image processing algorithms to be discussed in detail in Sec. IV. These films were sputter deposited on single-crystal Si to a nominal thickness of 100 nm in an ultrahigh vacuum chamber at Lehigh University, and thinned to electron transparency using a chemical etch. TEM and STEM micrographs were acquired using a Philips 400T TEM/STEM at 120 kV, and these images were used as the basis for comparison between conventional image processing and the newly developed processing methodology. Conventional image processing was performed on a Macintosh computer using the public domain NIH IMAGE program (W. Rasband, U.S. National Institutes of Health).

Once the testing of the improved processing methodology was complete, optimized plan view TEM images of the grain structure of a uniformly thin Al film were analyzed both manually and automatically to extract the grain size distribution. The Al film was sputter deposited to a nominal thickness of 30 nm on single crystal NaCl at the IBM T.J. Watson Research Center in Yorktown Heights, NY. The sample was annealed for 30 min at 450 °C under flowing Ar–4% H_2 in a tube furnace at Lehigh University, followed by air cooling. The film was removed from the substrate by dissolution and caught on a 3 mm TEM grid for analysis. Bright-field TEM images were taken on plate negatives using a 120 kV Philips 400T TEM/STEM with a LaB_6 source. An accelerating voltage of 80 kV was used, with a 200 μm condenser aperture and a 100 μm objective aperture, at a magnification of 13 000×.

These electron optical conditions were chosen to maximize grain-to-grain contrast and minimize problematic contrast mechanisms (e.g., bend contours, strain contrast, and boundary fringes) while maintaining good resolution. A full discussion of the optics and contrast in TEM is beyond the scope of this article, however the interested reader may refer to any text on TEM,[5,15] and a brief summary is presented in Appendix A. The magnification was chosen to maximize the number of grains in each image, subject to the constraint that the smallest grains must still be easily traced from a 3×-magnified positive print.

The contrast between neighboring grains varies as the specimen is tilted, but at any given tilt, a large number of boundaries will be out of contrast. Micrographs were taken at four different specimen tilts for each field of view, typically separated by 1° or less to avoid significant foreshortening. The use of multiple tilt conditions ensures that the majority of boundaries appears in strong contrast at least once. This is especially important if there are regions which contain large areas of small grains separated from each other by very low angle boundaries, as is often the case in fiber textured metal films. Such regions may appear uniform over many degrees of tilt, until some critical tilt is reached at which the smaller grains appear distinct from each other.

Manual analysis was performed by tracing grain boundaries from the positive prints onto transparencies. After locating the boundaries from one micrograph, the transparency was overlaid on the next micrograph from the same field of view, using recognizable features to correct for translational offsets between images. Additional boundaries were traced onto the same transparency and the process repeated for each micrograph of the field of view, resulting in a single tracing representing the boundaries detected in four micrographs. Each transparency was then scanned into an image file at a resolution of 203 pixels/in., corresponding to 307 pixels/μm after scaling for magnification. The resulting file was skeletonized to reduce the grain boundaries to features of single-pixel width, and the grain size distribution was measured from this binary image. Tracing the grain structure took about 4 h for each field of view (comprising four images), and subsequent extraction of the grain size distribution took ~0.5 h, with an average yield of ~1500 grains from each field of view.

Automated analysis was performed on a Digital AlphaStation 433 using digitized 8-bit grayscale images (256 different gray values) which had been scanned directly from the negatives at a resolution of 600 pixels/in., corresponding to 307 pixels/μm. Using four images from each field of view, grain boundaries were located automatically by the algorithm discussed in Sec. IV, and the grain size distribution was extracted from the resulting binary image. The entire process took about 1.5 h of processor time, and had an average yield of ~800 grains from each field of view.

IV. IMAGE PROCESSING METHODOLOGY

Ideally, the image processing sequence should extract the maximum amount of reliable information from the input

image with minimal inclusion of spurious features. It is also necessary to minimize the introduction of artifacts during various steps of the processing itself, and if full automation is to be achieved, this must be done without reliance upon the user to make critical decisions. The process applied to Fig. 3(A) violates all of these guidelines, so clearly it is not appropriate for the current task. This does not imply, however, that the components of conventional image processing are inapplicable. Rather, by employing many of these methods in an optimal order, and combining them with newly developed techniques, we will show that many of the shortcomings evident in Fig. 3(B) can be mitigated. Such a strategy requires, however, an appreciation of the strengths and limitations of conventional image processing methods (e.g., noise filters, edge filters, thresholding, and various binary operations) as applied to TEM images. These methods are reviewed in some detail in Appendix B, and may also be found in typical texts on image processing.[10]

A. General overview

1. Design philosophy

As illustrated by Figs. 3(A) and 3(B), the primary limitation of current image processing algorithms for the extraction of grain boundaries is the inclusion of incorrect information in the form of spurious features, even in high quality images, which results in a corrupted microstructural analysis. For this reason, it is of paramount importance to minimize or eliminate spurious features from the processed image. As a result, the efficiency of data extraction will be relatively poor, but this can be accommodated by the acquisition of multiple images taken at different sample tilts from each field of view. Our perspective is that the marginal increase in the microscopy effort is an acceptable trade off for reliable quantitative microstructural analysis, given that the task of identifying grain boundaries can be automated.

Although it is desirable to minimize the need for repetitive human intervention, this does not mean that all human inputs should be eliminated. In particular, many image processing steps (e.g., dilation, erosion, etc.) are facilitated by the incorporation of a characteristic microstructural length scale supplied by the user. The algorithm, to be described below, has proven to be robust under a variety of circumstances, but it should be remembered that the single most important consideration is the information content of the starting images.

2. Grain boundary detection algorithm

Building upon the strengths of existing image processing techniques, we have developed several additional techniques and integrated them into a methodology which adheres to the design philosophy outlined above. The overall algorithm, summarized in several flow charts shown in Fig. 4, will be explained briefly here, and followed (in Sec. IV B) by a more detailed discussion of the new processing techniques which have been developed. Multiple images of the same field of view are taken as input, along with the user-specified length scale, and each image is processed independently to extract high-contrast grain boundaries before optimal recombination.

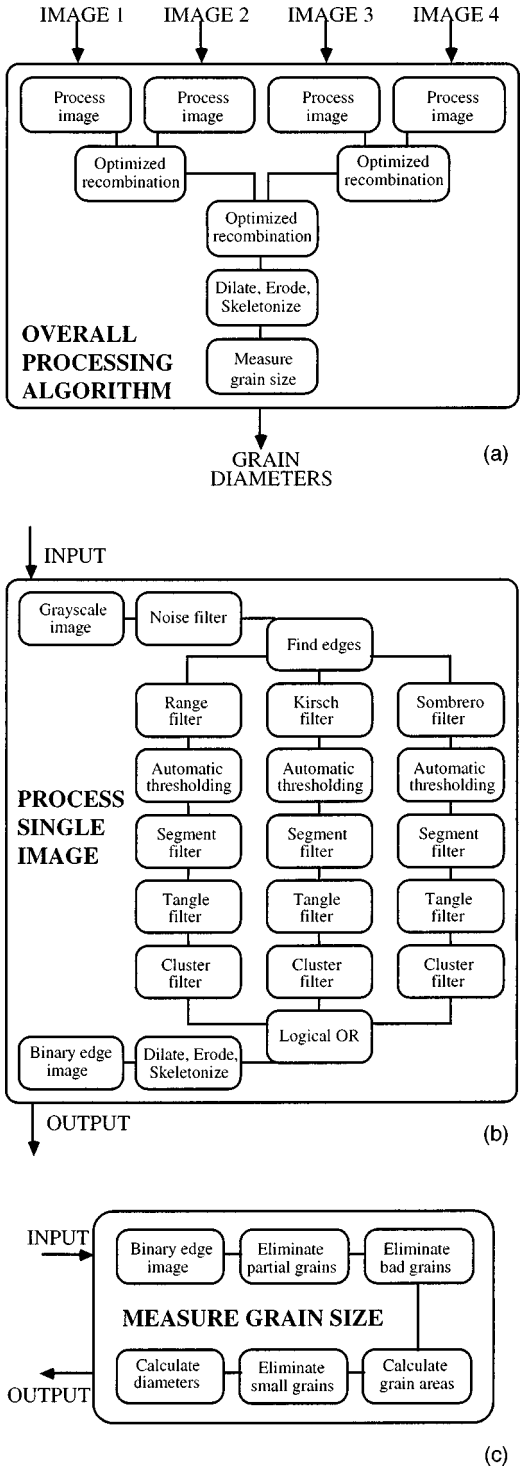

FIG. 4. Flow charts summarizing the improved microstructural analysis including (a) overall methodology, (b) single-image grain boundary detection algorithm, and (c) grain size measurement algorithm. Details of the new, specialized filters are discussed in Sec. IV B.

a. Single image processing. As a first step, noise reduction is performed on each image using a hybrid median filter,[16] resulting in a smoothed image which is amenable to edge detection. The current implementation employs three

typical edge filters, each of which detects a subset of edges in the image: A range filter with a 3×3 kernel, a 13×13 sombrero filter (also called a Mexican hat filter), and a 3×3 Kirsch filter.[17] A variety of other edge filters (e.g., Roberts Cross operator, Frei and Chen operator, etc.) may be found in Ref. 10. In general, a battery of edge filters should be selected based upon the type(s) of contrast exhibited by grain boundaries in the starting micrograph, allowing the algorithm to be tailored to various samples and/or microscopies. Following edge detection, each of the resulting images is independently processed with a series of operations to reduce it to a binary image containing only well-connected grain boundaries corresponding to high-contrast edges in the original image.

This reduction is achieved by automatic thresholding and skeletonization, followed by several filters designed to remove features which are likely to be spurious. Specifically, short, unattached line segments, overly connected (''tangled'') segments, and disconnected clusters are removed in sequence by their respective filters, as discussed in detail in Sec. IV B. The three binarized, filtered edge images, each containing a subset of grain boundaries, are recombined into a single image by a logical OR operation. Subsequent consolidation of edges is achieved using simple dilation, skeletonization, and erosion operations in sequence, leaving a binary image containing single-pixel lines at well-connected grain boundaries.

A comparison between the above methodology and a conventional methodology [similar to the one used to produce Fig. 3(B)] is shown in Fig. 5. The starting image [Fig. 5(A)] is a bright-field STEM image of a 100 nm, as-deposited pure Al film. The results of conventional image processing are shown in Figs. $5(B_1)$–$5(D_1)$. The image processing steps used to produce these images can be summarized as follows: Noise reduction (median filter), edge detection (Sobel operator), manual thresholding [Fig. $5(B_1)$], dilation, skeletonization, erosion [Fig. $5(C_1)$], a closing operation, and a final skeletonization [Fig. $5(C_1)$]. Results from the application of the improved algorithms to the same image are shown in Figs. $5(B_2)$–$5(D_2)$ at stages in the processing sequence which are comparable to those shown in Figs. 5 (B_1)–$5(D_1)$. As is evident from Fig. 5, the conventional approach locates the majority of the boundaries, but also includes a substantial number of spurious features. In contrast, the new algorithm locates only a subset of the boundaries, but almost entirely eliminates spurious features.

b. Multiple image recombination. The processed binary images resulting from different sample tilts at the same field of view may now be recombined into a single image. Unfortunately, this recombination is hindered by the imperfect registry of the images. This disregistry arises primarily from three sources: (1) Image translations during tilting, (2) analog image acquisition (e.g., plate film), and (3) image digitization (e.g., scanning). Several comments are in order here. First, image shifts during specimen tilting are unavoidable at high magnifications, even if the sample is properly located at the eucentric height of the microscope. Second, image translation and/or rotations may be introduced by misalignment of negatives during either image acquisition or subsequent digitization. Since it is estimated that rotations are on the order of 0.01 rad, this effect has been neglected. Given these considerations, the ideal instrument for our purposes would be a scanning transmission electron microscope (STEM) with beam tilt control and digital image acquisition. However, due to the limited availability of such instruments, a methodology has been developed to correct for arbitrary image shifts associated with a typical TEM configuration.

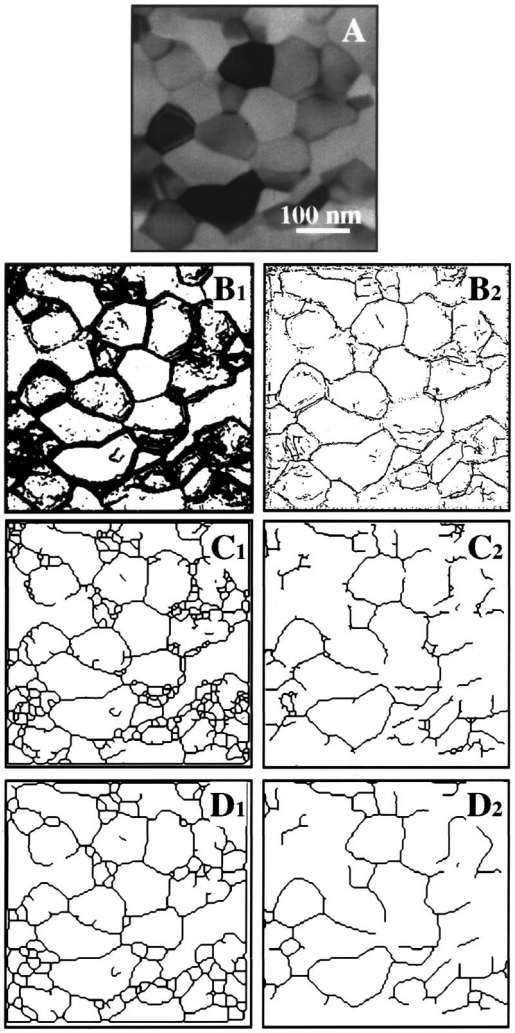

FIG. 5. (A) Bright-field STEM micrograph of a 100 nm Al film showing substantially improved contrast. (B_1)–(D_1) Results from conventional image processing, after (B_1) median filter and Sobel operator, (C_1) dilation, skeletonization, and erosion, and (D_1) closing operation and final skeletonization. (B_2)–(D_2). Results from improved image processing, after (B_2) hybrid median filter and Kirsch filter, (C_2) dilation, skeletonization, segment filter, and tangle filter, and (D_2) cluster filter and final consolidation. Note that while the grain boundary yield of the conventional processing is much higher, a substantial number of erroneous boundaries are detected, while very few such features are detected by the improved algorithm.

In our procedure, nonoverlapping pairs of processed images are recombined by the introduction of an optimum translation (determined by a process which will be discussed in Sec. IV B), followed by a logical OR operation. In short, an input set of 2^n images ($n=1,2,3,...$) is recombined into a single output image after 2^n-1 pairwise operations. Following recombination, a consolidation process consisting of dilation, skeletonization, and erosion steps is applied in order

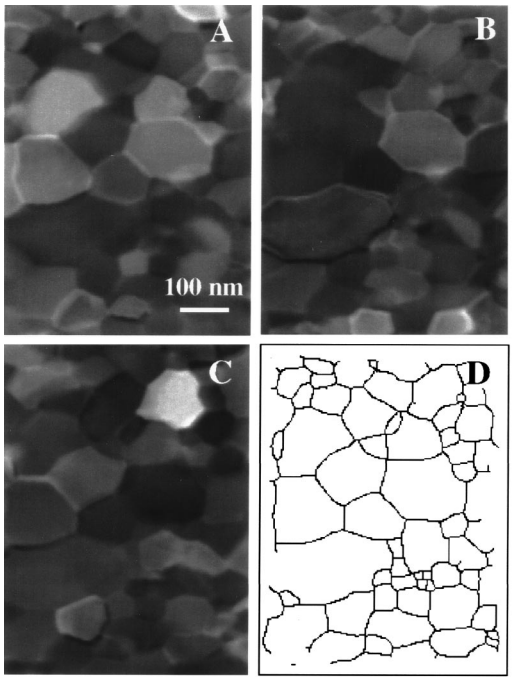

FIG. 6. (A)–(C) Bright-field STEM micrographs of a 100 nm Al film taken at different specimen tilts from the same field of view. Note the changes in contrast as a function of tilt, and the significant translations between images. (D) Composite image of detected grain boundaries based upon analysis of eight images from the same field of view using the improved grain boundary detection algorithm along with optimized image recombination. The boundaries detected in this image are ~95% reliable.

to improve the connectivity of the boundaries in the final image and make it amenable to grain size analysis.

The successful application of the grain boundary identification and optimized image recombination algorithms described above is illustrated in Fig. 6. Figures 6(A)–6(C) are STEM images of the same Al film shown in Fig. 5, each from the same field of view, but at different tilts. Each image shows strong contrast at a subset of grain boundaries, but also contains regions of low contrast where boundaries cannot be distinguished easily. In addition, it is clear that the images are translated with respect to each other by significant amounts (on the order of 1/4 of a grain diameter), making this set of images a good test case. The successful recombination of binary edge images from eight micrographs [including Figs. 6(A)–6(C)] is shown in Fig. 6(D), which is estimated to contain >95% of the boundaries present with minimal inclusion of spurious features.

c. Grain size determination. Measurement of the grain size distribution from the final binary image is accomplished easily, since the area of any enclosed region may be determined by simply counting the pixels within the boundaries. However, in order to ensure that only high-quality information is included in the final output, it is necessary to eliminate any suspect regions before the final analysis. Any region which touches the boundaries of the image is eliminated since it constitutes a fractional grain. Additionally, any region which contains a disconnected or broken segment is eliminated since these are assumed to be incomplete grain boundaries. After all such regions have been removed, the pixels inside of each closed region are counted to give an area, and these areas are converted into corresponding grain diameters (assuming circular grains, reasonable for an equiaxed structure). The final step is a conversion from pixels into units of actual length, based upon the pixel density and the known magnification of the starting image.

B. Detailed description of new algorithms

The following section contains a brief summary of each of the image processing algorithms which have been developed to assist in the automation of grain boundary identification.

1. Automated thresholding

As discussed above, a thresholding operation is required to reduce the grayscale edge image to a binary image and thereby allow subsequent binary operations such as dilation, erosion, and skeletonization. It is highly desirable to achieve repeatable, optimum thresholding without the need for human judgment since this process must be executed on every image to be analyzed. For this reason, we have developed a simple algorithm which thresholds a grayscale image based upon its histogram. The image histogram is generated by counting the number of pixels which have each of the possible values (typically 0 to 255) and plotting the number counted as a function of value. In general, the histograms of grayscale images produced by edge finding algorithms are monomodal and near-continuous in the region containing the peak. Assuming that these conditions are met, the first step in the thresholding process is to smooth the histogram so that its derivatives will be well-behaved. The first and second derivatives are calculated using a central-difference technique, and the inflection point following the peak maximum is located. This inflection point is a convenient threshold value since it is can be easily located on any well-behaved histogram, independent of absolute peak position or peak width. When this value is used in the thresholding step, empirical comparisons show that only a very small fraction of resulting features are spurious. While some information is lost which would have been retained if a human were to choose the threshold value by inspection, this loss of efficiency is deemed an acceptable trade off in order to eliminate the need for human intervention.

2. Segment filter

Once the image has been thresholded as described above, it is desirable to remove any short, disconnected line segments as they are likely to be spurious. Initial efforts to achieve this using an erosion process were of very limited utility because its inherent lack of selectivity results in the shortening of all disconnected segments, including those which are expected to be ''real.'' Unfortunately, once these segments have been shortened, their restoration is difficult, and repeated erosion will often result in unnecessary boundary elimination. Clearly this is an undesirable situation, and it would be preferable to remove short, disconnected segments without affecting longer, well-connected segments. This has been accomplished by testing each black pixel in the binary image to determine whether it belongs to a segment of some minimum length, specified here by the user to

be the estimated length, in pixels, of the shortest real grain boundary segment in the image (e.g., 15 pixels for the current set of images).

A simple method for identifying short segments is to start a random ''walker'' at each black pixel in the image which is constrained to move only upon black pixels. After each iteration, the distance from the walker to its initial position is determined and, once the walker has traveled some specified distance, the segment is considered to be sufficiently long and may therefore be retained. Conversely, if the walker is never able to travel the required distance, even after a large number of steps, then its starting pixel belongs to a short segment, and is removed from the image. The diffusive nature of this process implies that the distance traversed scales with the number of steps to a power less than unity, so a large number of steps is required to properly sample segment length. Some improvement may be realized if the walker is biased so that it will continue to move in the same direction as long as possible. However, even with this modification, a fundamental limitation of this approach is that the number of steps taken is unnecessarily large, and so this stochastic algorithm, while viable, is rather inefficient.

A more elegant approach constrains the walker to a systematic path, and is similar in spirit to conventional maze-solving algorithms. In this case, the walker attempts to move in a direction as close as possible to that of its last step, backtracking only if no suitable forward path is found. This approach requires line segments of single pixel width, allowing one to replace distance with the number of forward steps as a descriptor of the walker's trajectory. By contrast with the random walker approach, this algorithm is fully deterministic, and is extremely efficient. One limitation of the directed walker approach, though, is that any closed loop will be considered a long segment, even if total perimeter of the loop is smaller than the user-specified distance, since the walker will simply continue to walk around the loop. However, small loops which are fully disconnected from other features are easily removed in a subsequent step, so this shortcoming does not represent a significant problem. Because of the substantial gains in efficiency, the current segment filter utilizes the directed walker method.

3. Tangle filter

This filter is essentially a specialized application of the segment filter discussed above. Its purpose is to eliminate line features which exhibit excessive connectivity, as such features are most likely to be spurious. Several such over-connected regions can be seen in Fig. 3(B) in places where the original image had, for example, a high concentration of fringes or bend contours. After processing, these regions typically consist of a large number of very short, well-connected segments, and resemble a tangled mass of string. If the pixels at the junctions between all line segments are removed by means of a specialized erosion operation, what remains is a large number of short, disconnected segments in the tangled regions, with other regions of the image essentially unchanged. The segment filter may now be applied, followed by a dilation operation to reconnect the surviving boundary segments. The result is the removal of only the tangled regions with minimal impact elsewhere.

4. Cluster filter

This filter is perhaps the simplest of our newly developed algorithms, and is used to remove small, completely disconnected features from a binary image. Although the segment filter is well-suited to removing line features, it cannot remove closed loops (as discussed above), and can also be confounded in other special cases. Often, localized features within grains which do not correspond to grain boundaries (e.g., precipitates, dust particles, dislocation clusters), may escape both the segment filter and the tangle filter. The retention of such features implies that some fraction of real grains will be lost during the final grain size analysis, so we have developed a technique to selectively remove them. This is accomplished by first defining a neighborhood with a diameter slightly greater than the characteristic size of the offending features (estimated using the user-specified length scale). If nothing intersects the boundary of the neighborhood, it is colored white. This will eliminate any feature which is fully contained inside the region, but will not cause the elimination of any connected boundary segments or larger features. This process is repeated at every pixel in the image, and may be applied multiple times in succession with neighborhoods of varying sizes.

5. Optimized image recombination

The logical OR function is a very simple method of binary image combination, but is only strictly applicable when the two images are known to have no translational or rotational offsets. If these conditions are not met, the OR operation will result in an image which does not properly represent either of the two starting images. As discussed above, the effect of relative image rotations is small and will be neglected. However, the problem of translational offsets is an important one and must be handled properly. We have chosen to quantify image registry using a parameter, ϕ^2, defined analogously to the conventional χ^2 statistic.[18] Here, ϕ^2 represents the sum of the squared distances from black pixels in image A to their corresponding nearest-neighbor black pixels in image B. This quantity is then minimized with respect to relative image position. The optimum offset is subsequently applied to image A before a logical OR operation is performed to combine both images.

It is assumed that ϕ^2 is well-behaved, with a single, global minimum relatively near the starting position in this two-dimensional parameter space. This is generally the case, as shown in Fig. 7, allowing us to place reasonable limits on two key parameters, the maximum image offset and the maximum relevant nearest neighbor distance. Since typical image offsets are ± 10 pixels in x and y, we restrict our maximum offset to a range of ± 50 pixels, and the nearest neighbor search distance to ± 15 pixels. These assumptions substantially reduce the computational burden associated with the minimization of ϕ^2. To further reduce this burden, we first calculate ϕ^2 at widely spaced positions distributed evenly over the entire range of possible image offsets (± 50

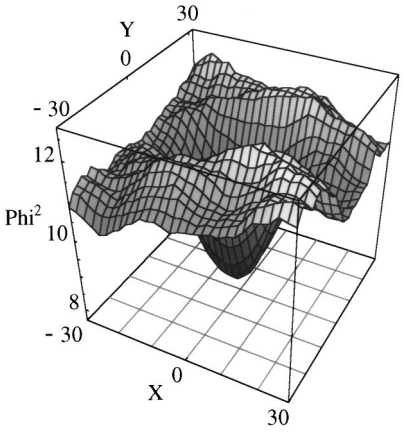

FIG. 7. Typical ϕ^2 surface as a function of relative image position (in pixels), used to quantify goodness of fit between images. The surface has a single, well-behaved, global minimum at (5, −6) pixels, corresponding to the optimum relative translation between the two input images. The depth of the primary minimum is less than would be expected for perfect registry due to missing boundary segments in each image.

pixels in x and y), selecting the position which gives the minimum value of ϕ^2. The value of ϕ^2 is then calculated for each of the eight neighboring positions, and the position which results in the largest decrease in ϕ^2 is selected. This process is repeated until the minimum is located, corresponding to the optimum translation between the two images in question. Other techniques, such as conjugate-gradient minimization,[19] are, of course, also possible, but have not been implemented here due to the difficulty of expressing ϕ^2 analytically.

V. RESULTS AND DISCUSSION

The algorithm discussed above has been used to automatically identify 8185 grains from optimized TEM micrographs of nine fields of view (36 micrographs). A subset of two fields of view (8 micrographs) was also analyzed manually to allow direct one-to-one comparison between the two methods. A portion of one of the analyzed micrographs is shown in Fig. 8(A), in which the grain-to-grain contrast has been improved at the expense of spatial resolution. In terms of image quality, the optimized TEM images fall somewhere between the typical TEM and best-case STEM images shown in Figs. 3 and 6, respectively, making them a good test case for the application of the new image processing methodology.

Probability distributions for all data sets were extracted and fitted (by an unweighted, least-squares method) to the lognormal distribution

$$p(x)=\frac{1}{\beta x\sqrt{2\pi}}\exp\left(\frac{-(\ln x-\alpha)^2}{2\beta^2}\right), \tag{1}$$

where α and β are independent fit parameters. The probability distribution of diameters from 8185 grains is shown in Fig. 8(B), along with a best-fit lognormal distribution. Two convenient parameters which reflect the gross shape features of the distribution are the mean and the standard deviation, given by

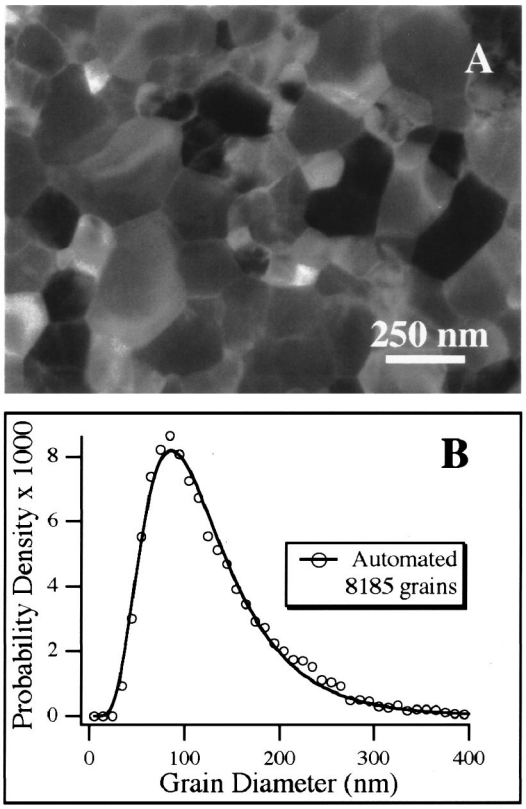

FIG. 8. (A) Optimized TEM micrograph of a 30 nm Al film which is representative of the images used as input to the automated grain identification algorithm. (B) Probability distributions of equivalent grain diameter from an automatically analyzed population of 8185 grains. The smooth curve is the best-fit lognormal distribution.

$$\mu=\exp(\alpha+\beta^2/2), \tag{2}$$

and

$$\sigma=\exp(2\alpha+\beta^2)\exp(\beta^2-1), \tag{3}$$

respectively. It should be noted that while the lognormal distribution appears to fit the data quite well, its use here is primarily empirical.

A comparison of the hand-traced and automatically determined distributions is shown in Fig. 9(A), from which it is evident that the two methods give very similar results over relatively large data sets. Two statistical measures of the goodness-of-fit have been applied, the chi-square test and the Kolmogorov–Smirnov (KS) test.[18,19] In each case, a parameter (e.g., χ^2 or D) is determined that is large for a poor match and zero for a perfect match, and subsequently used to calculate the statistical significance of the difference between the data sets. The significance ranges from 0 to 1, and represents the probability that two sets drawn from a common distribution will have χ^2 or D greater than the one observed.

The chi-square test, applied to the 40 bin histograms shown in Fig. 9(A), resulted in a significance of 0.05, implying that they are quite different. However, the chi-square test is overly sensitive to noise in the histograms, especially in the tails, which means that the particular choice of bin size will be the dominant factor in determining whether the distributions are similar. For noisy data, the KS test is more robust than the chi-square test because it is applied to cumu-

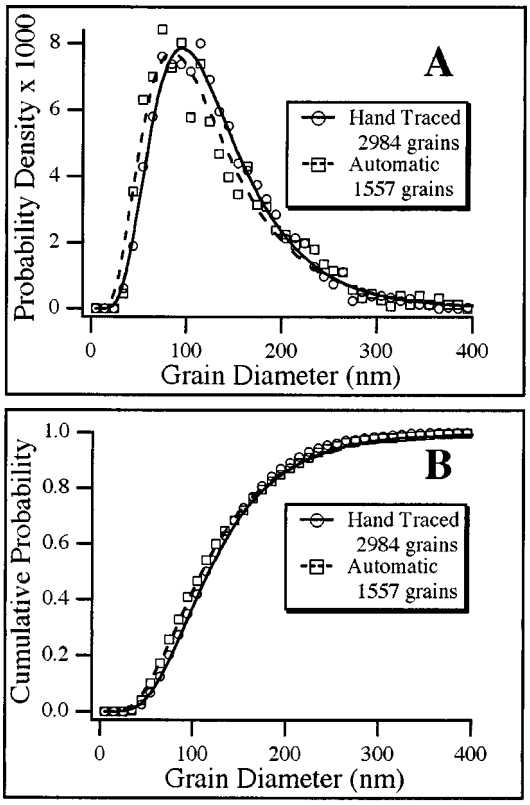

FIG. 9. (A) Probability distributions of equivalent grain diameter from manual and automatic analyses of identical micrographs (2984 and 1557 grains, respectively). (B) Cumulative probability distributions generated from the same data and using the same bins as in (A). Smooth curves correspond to best-fit lognormal distributions.

lative distributions instead of frequency distributions. Therefore, the KS test was applied to 40 bin [shown in Fig. 9(B)] and 200 bin cumulative distributions of the two data sets, resulting in significance values of >0.99 and 0.81, respectively. Therefore, the hand-traced and automatically determined cumulative distributions are not significantly different over populations of a few thousand grains, independent of the choice of binning parameters.

Having made this comparison, we now consider the first two moments of the three measured data sets, as determined directly and by lognormal fitting, which are summarized in Table I. The mean values over all three sets, and both calculation methods, agree within ~5%, while the standard deviations vary by up to 24%. In fact, the Student *t* test shows that

TABLE I. Means and standard deviations of the three measured grain size distributions, calculated directly from the data and from the lognormal fit parameters. The values for a particular data set and its fit will coincide if the dataset contains a sufficient population of grains and is lognormally distributed. Substantial differences occur in the second moment due to noise in the tails of the distributions.

Data Analyzed	Manual 2984 grains		Automatic 1557 grains		Automatic 8185 grains	
Method used	Direct	Fit	Direct	Fit	Direct	Fit
Mean (nm)	136	134	135	129	133	125
Std. dev. (nm)	59	67	67	73	66	67

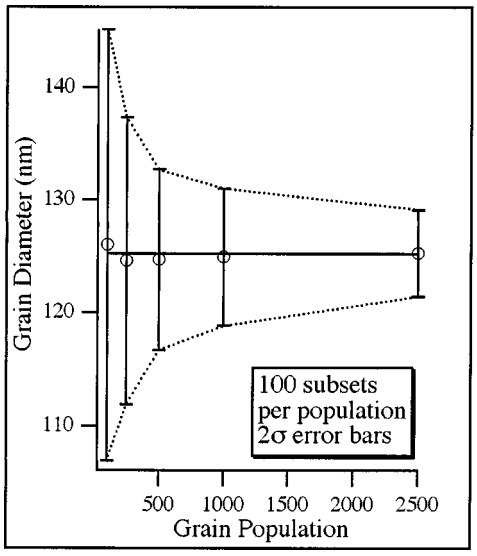

FIG. 10. Expected values of the mean, calculated from the lognormal fit parameters of 100 random subsets, plotted as a function of grain population *N*. The width of the 95% confidence interval (represented by error bars) decreases systematically with increasing *N*.

the means, as determined directly from the hand-traced and automatically determined data, agree at the 95% confidence level, whereas the *F* test shows that the variances are significantly different at the same confidence level. Disparities in these variances may be expected since higher-order moments are more sensitive to noise, especially in the tail of the distribution.

It should be noted that potential sources of error are numerous, and include, but are not limited to, incorrect location of grain boundaries, finite pixel size, the assumption of equiaxed grains, and problems associated with the microscopy used to generate the starting images, e.g., drift, defocus, etc. In addition, for manual analysis, the actual determination of what constitutes a grain boundary is nontrivial, often somewhat ill-defined, and strongly variable from person to person.[20] Thus, a significant advantage of the automated approach is that criteria for identifying a boundary are well-defined and entirely consistent.

Finally, we return to the question, considered in Sec. I, of determining what constitutes an adequate grain population. We consider here the dependence of the mean grain size on sample population from random subsets chosen from a total of 8185 grains. For each sample size ($N=100$, 250, 500, 1000, and 2500 grains), 100 independent probability distributions were compiled, and the mean grain size was calculated for each distribution based upon a lognormal fit. For each *N*, we obtained the expected value of the mean at the 95% confidence level. These data are summarized in Fig. 10, which clearly shows a decrease in the widths of the confidence intervals with increasing *N*. Specifically, the relative error in a single measurement of *N* grains drops from $\pm 15\%$ to $\pm 5\%$ as *N* increases from 100 to 1000 grains, implying that conclusions based on ~100 grains should be interpreted with a great deal of care. For some critical applications, such as semiconductor process control and/or development, this improvement in precision can be very significant.

Based upon the foregoing analysis, the optimum sample size for this material system is 500–1000 grains, since counting additional grains has negligible impact on the results. In this case, the grain size distribution is well-behaved and monomodal. If, however, the exact behavior at the tails of the distribution is of interest (as is often the case for magnetic thin film media), or if some abnormal grain growth has occurred, this sampling might be insufficient.

VI. CONCLUSIONS

New algorithms have been developed which, in conjunction with existing image processing algorithms, make fully automated microstructural analysis of TEM micrographs feasible. This has been facilitated by the optimization of image contrast, the acquisition of multiple images from each field of view at different sample tilts, and the incorporation of a single, user-estimated characteristic length scale from the microstructure. A quantitative, statistical analysis has shown that the results of this automated technique agree very well with those of a conventional, manual approach. A particular strength of the automated approach is that it is entirely predictable and consistent, eliminating the unavoidable subjectivity involved with manual delineation of grain boundaries. While the emphasis of this work has been on the processing of TEM images, the methodology which has been developed should also be applicable to other types of images which show similar contrast (e.g., FIB), and may be suitable for analysis of other types of images (e.g., atomic force, or scanning electron) with some relatively small modifications.

ACKNOWLEDGMENTS

One of the authors (D.T.C.) gratefully acknowledges support from the NSF in the form of a Graduate Research Traineeship under Grant No. DMR-9256332. Two of the authors (K.B. and J.M.R.) gratefully acknowledge support from NSF under Grant No. DMR-9713439. The authors especially wish to thank Professor D. B. Williams for his input and encouragement. Thanks also to G. A. Lucadamo, V. J. Keast, M. Watanabe, and D. W. Ackland for fruitful discussions and technical assistance.

APPENDIX A: SOURCES OF CONTRAST IN TEM IMAGES

Since the signal in a TEM consists of electrons hitting some detection device, sources of contrast comprise anything which affects the electron intensity reaching the detector. The simplest mechanism is mass-thickness contrast, changes in electron intensity due to changes in the average atomic number or the thickness of a sample. Since the electrons must pass through the entire thickness of the specimen to reach the detector, it is clear that thicker regions will appear darker because more of the electrons will fail to pass through. Similarly, since heavier elements absorb electrons more readily, regions of high atomic number will also appear darker than regions of low atomic number. This contrast mechanism is always present, and the effects of changes in the mass and thickness cannot be separated from each other reliably.

The second major mechanism is diffraction contrast, which arises from the systematic reflection of electrons by an ordered array of atoms. When a single grain happens to fulfill Bragg's law, it will tend to diffract most of the incident intensity by a large angle and therefore such a grain would appear dark in a bright-field image. Boundary fringes, strain contrast, and bend contours are all essentially special cases of diffraction contrast which arise under certain circumstances, and for our purposes they are all detrimental. Boundary fringes are sharp features which appear in tilted boundaries or other planar defects. Strain contrast arises in areas where the lattice parameter has effectively been changed by deformation, causing the local region to diffract under different conditions from the matrix. Bend contours arise due to bends in the specimen which change the apparent angle of incidence of the electron beam, again causing differences in the diffraction behavior locally. All of these sources of contrast can be active at once, and it is generally impossible to separate them from one another after the fact.

In order to find grain boundaries, we generally rely upon differences in the diffraction conditions between neighboring grains to result in an overall intensity difference between them. This is a subtle effect, and is very easily overshadowed by any of the other contrast mechanisms which may be active. For this reason, it is necessary to do everything possible to prevent nonbeneficial contrast mechanisms from being active. In general, mass-thickness contrast will not be problematic for most systems as long as there are no fast changes in thickness or composition. However, strain contrast and bend contours can easily be mistaken for real boundaries by image processing software, and should therefore be avoided if at all possible. This must be done by very careful specimen preparation and handling to minimize the addition of any bends or strains to the specimen.

It is generally desirable to minimize the effects of diffraction contrast in the images, and this can be done in a variety of ways. The simplest of these is to use a STEM which reduces diffraction contrast inherently due to the large convergence angle of the focused electron probe. However, since STEMs are not extremely common, it is helpful to also present some guidelines for minimization of diffraction contrast in the conventional TEM. It is best to work in a condition where there are many strong diffracted beams since boundary fringes, bend contours, and strain contrast are weakest under these conditions. The strength of these diffraction effects can further be minimized by adjusting the microscope optics to give a large convergence angle and a large acceptance angle in the backfocal plane (i.e., a large condenser aperture and a large objective aperture), although this is done with some loss of image resolution due to increased aberrations. Last, operating at lower accelerating voltages will increase the apparent angular spread of the objective aperture and appears to strengthen the weak contrast between grains to a limited extent. These conditions represent at least a starting point for improving the quality of TEM images so that they may be processed more reliably but, as is always the case in TEM analysis, nothing works well all of the time, and every material system should therefore be treated individually to find what works best.

APPENDIX B: CONVENTIONAL IMAGE PROCESSING

Most image processing algorithms operate on a spatially localized region in an image, often called a neighborhood. An example of such an operation would be the convolution of a kernel with an image. Each pixel in the image can be treated as the central pixel in its neighborhood (ignoring those pixels near the edges), and the kernel is a matrix which supplies weighting factors for each of the pixels in the neighborhood. The central pixel is replaced by the weighted average of the neighborhood pixels as specified by the kernel. In this way, a large number of operations may be applied by simply adjusting the weighting scheme of the kernel, including smoothing, top-hat filtering, etc. However, this approach is not sufficient for all tasks since it is not always possible to design a kernel which will have the desired effect. Many other operations maintain the idea of a neighborhood, but are more complex than a simple convolution. With this in mind, the most common grayscale image processing operations applicable to the problem of locating grain boundaries will be discussed briefly below, followed by binary operations, with an emphasis on the relative strengths and weaknesses of each.

1. Grayscale operations

a. Noise filters

Since most images contain noise of some sort, it is generally necessary to smooth them or otherwise remove the noise before more complex filters are applied. Smoothing may be achieved by the convolution of a kernel, typically with values corresponding to a Gaussian about the central pixel. While this approach does a good job of noise reduction, it also results in the blurring of features over a distance proportional to the size of the neighborhood. Significant noise reduction requires relatively large neighborhoods, and the blurring introduced is detrimental to subsequent edge-finding operations. An alternative is the median filter, which takes a neighborhood and finds its median value, then substitutes that value into the central pixel. This operation is most often used to eliminate spot noise from grayscale images, however it still has the effect of blurring edges and rounding corners, and repeated application can result in significant information loss. The benefit of using a median filter instead of a Gaussian smoothing kernel is that more noise reduction can be achieved within a smaller neighborhood with the median, thereby limiting the magnitude of the blurring introduced.

b. Edge filters

Edge filters employ kernels which are sensitive to local spatial variations, and their application leads to information as to the relative strengths of edges. For instance, a region containing a sharp, black to white transition will have a high value, and a region of uniform intensity will have a value of zero. In all cases, the end result is a grayscale image where large values correspond to strong contrast. A very simple approach to finding edges is the range filter, which simply calculates the difference between the maximum value and the minimum value within a neighborhood, and substitutes that difference into the central pixel. This filter works reasonably well if the neighborhood is small and the image is noise-free, whereas in noisier images the range approach breaks down entirely. The Sobel filter finds edges by calculating the spatial derivatives across the central pixel in the neighborhood in two orthogonal directions. The central pixel is then replaced by the sum in quadrature of these derivatives. This approach makes the Sobel operator quasi-isotropic and sensitive to small gradients as well as large ones, but many such small gradients in TEM images are actually spurious.

Another approach based on spatial derivatives is the Kirsch filter which compares the magnitudes of the spatial derivatives along all the directions in the neighborhood. The central pixel value is replaced by the maximum of these derivatives. This operator gives results similar to those resulting from the application of the Sobel operator, but is not as sensitive to small gradients. Edges may also be located by convolution with a Laplace kernel, which is essentially a discretization of the Laplacian operator. As with the previous filters, it is well-suited to finding high-contrast edges, but is less effective at finding the subtle ones. Thus, the ability to locate real edges in TEM images with good sensitivity, but without the inclusion of spurious features, is clearly nontrivial.

c. Thresholding

Thresholding allows some subset of image pixels to be selected based upon their values. In the simplest case, the value of each pixel in the image is compared to a threshold value. Any value less than the threshold value is set to white, while all others are set to black. This selects only those pixels whose values were larger than the threshold, and additionally has transformed the grayscale image to a binary one. This step is required if any binary operations (discussed below) are to be applied. However, in general, the threshold value must be specified by the user, and information is invariably lost in the transformation. When attempting to locate grain boundaries, thresholding is applied after potential edges have been found by one or more of the above methods. The primary difficulty involved with thresholding in this case is the inclusion of low-contrast edges. If the threshold is set so that only the very high-contrast edges are selected, a very large fraction of the total information is lost. However, if the threshold is set to select low-contrast edges, there is an increasing likelihood that spurious information will be included. This is an unavoidable trade off, and some consistent approach is required in order to make a fully automated process possible.

2. Binary operators

Once the grayscale image has been thresholded (ideally to select only those features which correspond to real grain boundaries), a variety of operations may be executed which exploit binarization. In the current case, black pixels correspond to grain boundaries.

a. Dilation and erosion

The process of systematically adding black pixels to an image is usually referred to as dilation, since it enlarges black features. This is achieved by applying the rule that any white pixel with at least N black neighbors will become black, where N is a user-specified integer. The main advantage of the dilation is that it can connect nearby black features (e.g., line segments corresponding to neighboring boundaries) and fill very small regions (e.g., small white spaces trapped by boundaries at a triple point). However, excessive use may cause spurious connections to arise between features, and can cause larger, enclosed areas (i.e., small grains) to be erroneously filled. The complementary operation, called erosion, is simply the inverse, where any black pixel with at least N white neighbors will become white. Erosion may be used to eliminate poorly connected black pixels from the binary image, under the assumption that such pixels are spurious. However, the drawback is that often there are poorly connected pixels which correspond to real features, and these will be lost as well.

b. Skeletonization

A special case of erosion, usually referred to as skeletonization, is the repeated removal of black pixels from all features until they reach single pixel thickness. This allows the reduction of thick lines to thin ones, which is often desirable after dilation steps. However, this operation is very sensitive to the exact shape of a region to which it is being applied, and the inclusion of a single white pixel into a black region will result in a new closed shape. This is clearly problematic since this means that the introduction of additional ''grains'' to the structure is quite easy.

c. Opening and closing

A series of N erosions, followed by N dilations is referred to as an opening operation since it tends to erase thin features which may enclose certain regions, effectively opening them up to neighboring regions. The complementary operation of N dilations followed by N erosions is called a closing operation since it tends to result in the complete filling of small, closed regions. These operations are typically used to selectively eliminate particular types of features, though this selectivity is imperfect, and the results are sometimes unpredictable.

d. Logical operations

Finally, binary images may be created or altered from one or more input binary images using pixel-by-pixel logical operations (e.g., AND, OR, NOT, etc.) since each pixel has a value of one (black) or zero (white). The AND operation will only color a pixel black if that pixel is black in all input images, while the OR operation only requires the specified pixel to be black in one input image. The NOT operation is equivalent to the inversion of a single input image. These operators are often used to combine binary images according to simple rules, although in theory there is nothing to prevent the construction of very complex rules for image creation or combination.

[1] E. E. Underwood, *Quantitative Stereology* (Addison–Wesley, Reading, MA, 1970).
[2] M. Berman, L. M. Bischof, E. J. Breen, and F. M. Peden, Mater. Forum **18**, 1 (1994).
[3] E. D. Schmitter, Steel Res. **66**, 449 (1995).
[4] R. Chinn, J. Am. Ceram. Soc. **77**, 589 (1994).
[5] D. B. Williams and C. B. Carter, *Transmission Electron Microscopy: A Textbook for Materials Science* (Plenum, New York, 1996).
[6] J. D. Mis and K. P. Rodbell, Mater. Res. Soc. Symp. Proc. **309**, 395 (1993).
[7] D. B. Knorr, D. P. Tracy, and K. P. Rodbell, in *Defect Structure, Morphology, and Properties of Deposits*, edited by H. Merchant (The Mineral Metals Materials Society, Warrendale, PA, 1995), p. 323.
[8] K. Barmak, R. A. Ristau, K. R. Coffey, M. A. Parker, and J. K. Howard, J. Appl. Phys. **79**, 5330 (1996).
[9] J. E. Palmer, C. V. Thompson, and H. I. Smith, J. Appl. Phys. **62**, 2492 (1987).
[10] J. C. Russ, *The Image Processing Handbook* (Chemical Rubber, Boca Raton, 1995).
[11] J. C. Russ and J. Christian Russ, J. Microsc. **148**, 263 (1987).
[12] K. Sakaue, ISIJ Int. **30**, 475 (1990).
[13] C. A. Lindley, *Practical Image Processing in C* (Wiley, New York, 1991).
[14] A. Rosenfield in *Digital Image Processing Techniques*, edited by M. P. Ekstrom (Academic, New York, 1984).
[15] L. Reimer, *Transmission Electron Microscopy* (Springer, Berlin, 1993).
[16] A. Nieminen, P. Heinonen, and Y. Nuevo, IEEE Trans. Pattern. Anal. Mach. Intell. **9**, 74 (1987).
[17] R. Kirsch, Comput. Biomed. Res. **4**, 315 (1971).
[18] R. von Mises, *Mathematical Theory of Probability and Statistics* (Academic, New York, 1964).
[19] W. H. Press, B. P. Flannery, S. A. Teukolsky, and W. T. Vetterling, *Numerical Recipes in C: The Art of Scientific Computing* (Cambridge University Press, Cambridge, 1988).
[20] D. T. Carpenter, J. R. Codner, K. Barmak, and J. M. Rickman (unpublished).